

From Particles to Fields: Reframing Photon Mapping with Continuous Gaussian Photon Fields

Jiachen Tao^{†1,2}, Benjamin Planche^{‡2}, Van Nguyen Nguyen^{‡2}, Junyi Wu^{†1,2},
Yuchun Liu², Haoxuan Wang¹, Zhongpai Gao², Gengyu Zhang¹, Meng Zheng²,
Feiran Wang¹, Anwesa Choudhuri², Zhenghao Zhao¹, Weitai Kang¹, Terrence
Chen², Yan Yan¹, and Ziyang Wu²

¹ University of Illinois Chicago, Chicago, IL, USA

² United Imaging Intelligence, Boston, MA, USA

Abstract. Accurately modeling light transport is essential for realistic image synthesis. Photon mapping provides physically grounded estimates of complex global illumination effects such as caustics and specular–diffuse interactions, yet its per-view radiance estimation remains computationally inefficient when rendering multiple views of the same scene. The inefficiency arises from independent photon tracing and stochastic kernel estimation at each viewpoint, leading to inevitable redundant computation. To accelerate multi-view rendering, we reformulate photon mapping as a continuous and reusable radiance function. Specifically, we introduce the **Gaussian Photon Field (GPF)**, a learnable representation that encodes radiance distributions as anisotropic 3D Gaussian primitives parameterized by position, rotation, scale, and spectrum. GPF is initialized from physically-traced photons in the first SPPM iteration and optimized using multi-view supervision of final radiance, encoding photon-based light transport into a continuous field. After optimization, the field enables differentiable radiance evaluation along camera rays without repeated photon tracing or iterative refinement. Extensive experiments on scenes with complex light transport, such as caustics and specular–diffuse interactions, demonstrate that GPF attains photon-level accuracy while reducing computation by orders of magnitude, unifying the physical rigor of photon-based rendering with the efficiency of neural scene representations.

Keywords: Neural Rendering · Neural Scene Representation · Photon Mapping · Differentiable rendering · Neural Radiance Field

[†] This work was carried out during the internship of Jiachen Tao and Junyi Wu at United Imaging Intelligence, Boston MA, USA.

[‡] Corresponding authors.

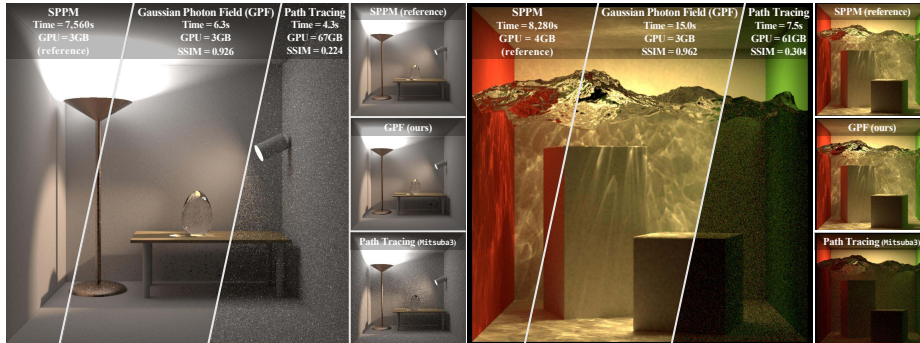


Fig. 1: Gaussian Photon Field (GPF) unifies photon mapping and neural field representations, achieving physically accurate, efficient, and view-reusable global illumination across diverse scenes, including indirect lighting (*left*) and water caustics (*right*). Using *Stochastic Progressive Photon Mapping (SPPM)* [12] and path tracing [17] as reference, our method produces substantially higher structural similarity (SSIM), while reducing rendering costs by orders of magnitude compared to SPPM.

1 Introduction

Accurately modeling light transport [21] is fundamental to realistic image synthesis, with applications in interactive graphics [4, 22, 47], medical imaging simulation [8, 34, 39], scene understanding via inverse graphics [1, 2, 49], *etc.* Physically-based rendering techniques [9, 37], such as photon mapping [18] and its variants [12, 13, 24], have long served as reliable estimators for complex global illumination, effectively capturing challenging phenomena such as caustics, indirect reflections, and refractions. Despite their accuracy, these methods remain computationally expensive when rendering multiple views of the same scene.

Prior work on photon mapping [18] addresses complex global illumination by decoupling light transport into two stochastic processes: photon tracing and density estimation. During photon tracing, photons emitted from light sources are stored upon surface and volumetric interactions, forming a global photon map. In the subsequent density estimation stage, the radiance at visible points is reconstructed by gathering nearby photons using spatial averaging based on stochastic kernel density estimation (KDE) [19, 35]. This formulation enables accurate estimation of caustics and diffuse inter-reflections, making photon mapping a robust estimator for a wide range of lighting phenomena.

However, photon mapping is fundamentally ill-suited for multi-view rendering. While photon tracing is view-agnostic and the photon map can be reused, storing millions or billions of photons is often impractical. More importantly, the radiance-gathering step is inherently view-dependent [12, 13, 18], requiring recomputation for each camera view. The kernel density estimate introduces view-dependent bias, as each view gathers a different subset of photons, causing flickering, brightness shifts, or blur. Increasing photon density reduces variance but raises memory and computation costs. Thus, the tight coupling between

visibility and per-view estimation makes classical photon mapping accurate but inefficient for multi-view reuse.

In contrast, modern neural scene representations, *e.g.*, neural radiance fields (NeRF) [28] and 3D Gaussian splatting (3DGS) [23], represent scene appearance and geometry as continuous functions that can be queried from arbitrary viewpoints. By learning such a shared representation, these methods amortize rendering costs across views. This motivates a fundamental question: **can photon mapping, traditionally a discrete, view-dependent estimator be reformulated as a continuous radiance field that encodes radiance distributions throughout the scene?** Such a formulation would enable consistent photon reuse across views, preserving the physical accuracy of photon mapping while achieving neural-style efficiency.

Toward this goal, we introduce the **Gaussian Photon Field (GPF)**, a learnable radiance representation that unifies photon mapping and neural field paradigms. GPF models the global photon distribution as a set of anisotropic 3D Gaussian primitives, each parameterized by its position, rotation, scale, and spectrum, forming a continuous and differentiable radiance field that can be queried from arbitrary viewpoints. Unlike traditional 3D Gaussian splatting, which represents view-dependent surface appearance, GPF encodes view-independent radiance distributions that capture global light transport phenomena such as caustics and indirect illumination. Once optimized, GPF enables efficient radiance evaluation along camera rays to render novel views, eliminating the need for repeated photon tracing, stochastic density estimation, or progressive refinement as in standard photon mapping. Conceptually, GPF replaces per-view KDE with a single, continuous photon-based radiance field.

We construct and optimize our Gaussian Photon Field in three stages: (1) Initialization: Gaussian primitives are initialized from photons traced in a single iteration of stochastic progressive photon mapping (SPPM) [12], providing a physically grounded starting point; (2) Radiance Query: a differentiable mechanism aggregates contributions from nearby Gaussians to estimate surface radiance, triggered at the first diffuse intersection after any specular or glossy bounces, at which point the ray terminates; (3) Supervision: the field is optimized end-to-end against reference radiance computed offline by SPPM, using sparse multi-view supervision. This process encodes complex, view-dependent light transport into a continuous, reusable radiance field.

To validate the effectiveness of our approach, we conduct extensive experiments across multiple physically-challenging scenes, including complex caustic and specular-diffuse interactions. We compare GPF against classical physically-based integrators (*e.g.*, path tracing [17] and SPPM [12]), Gaussian mixture fitting (EM-GMM [15]), neural scene representations (*e.g.*, NeRF [28], 3DGS [23], and AnySplat [20]), and feed-forward rendering (RenderFormer [46]). Measuring visual quality, render time, and storage cost, results confirm that GPF achieves photon-level accuracy with significantly reduced computational redundancy and successfully unifies the physical accuracy of photon-based rendering with the efficiency and scalability of continuous learned representations.

2 Related Work

Physically-Based Global Illumination. Simulating global illumination (GI) [21] is a central problem in computer graphics. Unbiased Monte Carlo methods, *e.g.*, path tracing (PT) [21] and its bidirectional variants (BDPT) [37], are considered the gold standard for accuracy. However, they struggle to efficiently sample complex, low-probability light paths, such as those that form caustics, often resulting in high variance and noise.

To address this, biased techniques like photon mapping [18] and its stochastic progressive variant SPPM [12] were developed. As detailed in Sec. 3, these methods excel at capturing complex GI phenomena by decoupling light transport into a two-pass process. Their primary limitation, however, is the *per-view estimation paradigm*, which fundamentally relies on a view-dependent kernel density estimation (KDE) process that must be re-executed for every new camera view. Our work directly targets this bottleneck. As illustrated in Figure 2, instead of proposing a new sampling strategy for these methods, we reformulate their core estimation process, replacing the repeated, per-view KDE with a query to a persistent, continuous radiance function.

Neural and Learned Scene Representations. The concept of a continuous, learnable scene representation was popularized by neural radiance fields (NeRF) [28]. NeRF and its many successors [5, 11, 25–27, 31–33, 36, 41, 42] achieve state-of-the-art novel view synthesis. However, these methods are essentially “black-box” appearance models: optimized for view interpolation, they lack physical grounding and cannot guarantee accurate light transport for complex effects such as caustics or relighting.

More recently, 3D Gaussian splatting (3DGS) [14, 23, 45] has achieved remarkable success, combining the efficiency of explicit primitives with the representational quality of neural scene models for real-time reconstruction. We draw inspiration from 3DGS in its use of Gaussians as compact, expressive primitives. However, our approach differs fundamentally in both objective and rendering process. While 3DGS models scene appearance and geometry through differentiable rasterization (splatting), our photon field represents the scene’s global illumination and radiance distribution arising from physical light transport. As shown in Figure 2, instead of rasterizing Gaussians to reproduce appearance, we employ them within a differentiable ray-tracing framework, where radiance is

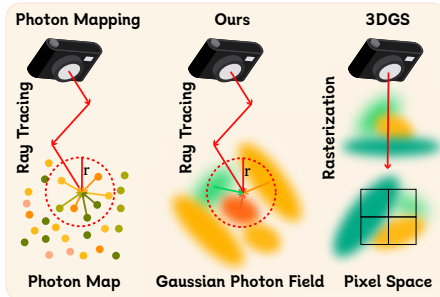


Fig. 2: Rendering paradigm comparison. Classical photon mapping estimates radiance by gathering discrete photons within a local radius r during ray tracing. GPF replaces this with a continuous, differentiable photon field queried via ray tracing. In contrast, 3DGS rasterizes primitives in pixel space, emphasizing appearance over physically-grounded light transport.

computed through continuous field queries. GPF thus extends Gaussian primitives to a physically-grounded domain, enabling efficient and reusable global illumination estimation across views.

Density Learning with Gaussian Mixtures. Gaussian mixture models (GMM) [6, 10, 15, 38, 43, 44, 50] have also been used to approximate light transport. Jakob *et al.* [15] proposed using Expectation-Maximization (EM) to fit Gaussian mixtures to photon distributions in *volumetric* participating media. Their derivation relies on a key property: a 3D Gaussian integrates to unity over 3D space, *i.e.*, $\int G(\mathbf{x})dV = 1$, enabling closed-form density estimation. However, this formulation does not transfer to *surface* photon mapping. For photons deposited on 2D manifolds, kernel density estimation requires $\int K(\mathbf{x})dS = 1$ over the surface. A 3D Gaussian does not satisfy this constraint, its integral over an arbitrary surface S depends on the position, orientation, and local geometry of S relative to the Gaussian, with no closed-form solution. Fitting 2D Gaussians in a global UV parameterization is also impractical for complex geometry with discontinuous or overlapping parameterizations. Our method differs fundamentally in 2 aspects: (1) **Learning target:** EM-GMM fits photon *density* and analytically derives radiance; GPF directly learns *radiance* via supervision. (2) **Optimization:** EM-GMM uses unsupervised EM; GPF uses gradient-based optimization with multi-view radiance supervision.

3 Preliminaries

Our work bridges classical light transport simulation with modern, learnable representations. To formally ground our method, we first review the rendering equation and then summarize the mathematics of progressive photon mapping—the paradigm we aim to reformulate.

3.1 Rendering Equation

Physically-based rendering aims to solve the rendering equation [21], a formulation of light transport in equilibrium. It states that the outgoing radiance L_o from a surface point \mathbf{x} in a direction ω_o is the sum of its emitted light L_e and all reflected incoming light:

$$L_o(\mathbf{x}, \omega_o) = L_e(\mathbf{x}, \omega_o) + \int_{\Omega} f_r(\mathbf{x}, (\omega_i)) L_i(\mathbf{x}, \omega_i) (\mathbf{n} \cdot \omega_i) d\omega_i, \quad (1)$$

where f_r is the bidirectional reflectance distribution function (BRDF) [30] describing the material, \mathbf{n} is the surface normal, Ω is the hemisphere of all incoming directions ω_i , and L_i is the incoming radiance at \mathbf{x} from direction ω_i .

The primary challenge in rendering is solving for L_i , as it is the solution to another rendering equation at the next surface intersection. This recursive integral is particularly difficult to solve for complex light paths, such as caustics, where high-energy contributions from a light source are focused onto a diffuse

surface after interacting with a specular (*e.g.*, glass or metal) surface. Unidirectional Monte-Carlo methods, *e.g.*, path tracing [21], struggle to sample these low-probability paths efficiently, leading to high variance.

3.2 Stochastic Progressive Photon Mapping

Photon mapping [18] and its progressive variants [12, 13] were introduced specifically to solve these difficult light paths. SPPM reformulates the problem by decoupling light transport into two passes.

Pass 1: Photon Tracing. In a view-independent pass, photons are traced from light sources till their interaction with non-specular surfaces. Each photon p records its position \mathbf{x}_p and flux $\Delta\Phi_p$, stored in a global spatial structure, *e.g.*, a k-d tree or hash grid, forming the photon map for subsequent density estimation.

Pass 2: Radiance Estimation. In a view-dependent pass, radiance is computed at all visible surface points $\{\mathbf{x}\}$ for the current camera. SPPM performs this using iterative kernel density estimation. In each iteration k , a search radius r_k is used to find nearby photons. Radiance is estimated by summing the flux of all N_p photons within the radius and normalizing by the kernel area:

$$L_i(\mathbf{x}) \approx \frac{1}{\pi r_k^2} \sum_{p=1}^{N_p} \Delta\Phi_p. \quad (2)$$

This radiance estimate is progressively refined by tracing more photons (increasing N_p) and shrinking the radius r_k , which allows the estimate to converge to a physically accurate result. Crucially, this process of gathering photons at a visible point and managing its local radius is fundamentally coupled to the camera view. It underpins the **per-view estimation paradigm** that limits photon mapping, whereas our method replaces it with a continuous, reusable function.

4 Method

4.1 Gaussian Photon Field Representation

Our method begins by recasting the discrete particle set of SPPM into a continuous, differentiable representation. Instead of a sparse point cloud, we introduce a Gaussian photon field (GPF), defined as a mixture of N anisotropic 3D Gaussian primitives, $\{\mathcal{G}_i\}_{i=1}^N$. Each primitive is parameterized as $\mathcal{G}_i = (\boldsymbol{\mu}_i, \mathbf{q}_i, \mathbf{s}_i, \boldsymbol{\Phi}_i)$, with a mean position $\boldsymbol{\mu}_i \in \mathbb{R}^3$, a rotation $\mathbf{q}_i \in \mathbb{H}$ (represented as a unit quaternion), a scale $\mathbf{s}_i \in \mathbb{R}_+^3$, and a spectral flux $\boldsymbol{\Phi}_i \in \mathbb{R}^3$. The rotation and scale collectively define the anisotropic covariance matrix $\boldsymbol{\Sigma}_i$. The radiance contribution G_i of a single primitive at any 3D point \mathbf{x} is then given by its un-normalized, flux-weighted Gaussian function:

$$G_i(\mathbf{x}) = \boldsymbol{\Phi}_i \exp\left[-\frac{1}{2}(\mathbf{x} - \boldsymbol{\mu}_i)^\top \boldsymbol{\Sigma}_i^{-1}(\mathbf{x} - \boldsymbol{\mu}_i)\right]. \quad (3)$$

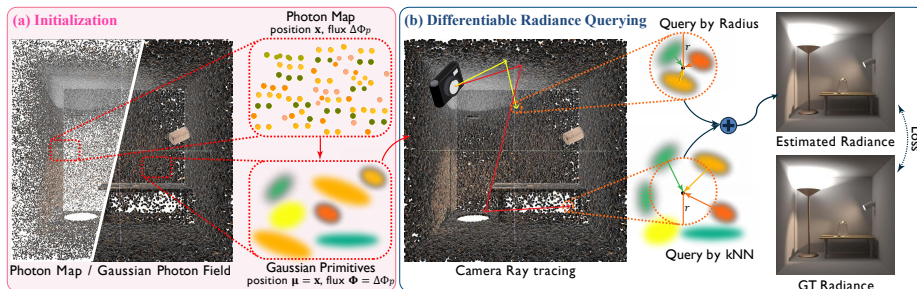


Fig. 3: Overview of the Gaussian Photon Field (GPF) pipeline. (a) **Initialization.** We convert the discrete photon map from one SPPM iteration into a continuous Gaussian photon field by instantiating one anisotropic 3D Gaussian per photon. Each primitive inherits the photon’s position and flux, with rotation and scale randomly initialized. (b) **Differentiable Radiance Querying.** During training and rendering, camera rays are traced through the scene. At the first diffuse intersection, radiance is estimated by aggregating contributions from nearby Gaussians via a radius-based and k-nearest-neighbor query. The predicted radiance is supervised by the GT values at corresponding surface points, enabling end-to-end optimization of all Gaussian parameters and producing a differentiable, view-reusable radiance field.

A key component of our method is its **physically-inspired initialization**. The GPF is not created from scratch, but directly seeded from classical simulation. We run a single iteration of SPPM to trace and store a sparse photon map. For each of the N photons p in this map, we instantiate one Gaussian primitive \mathcal{G}_i , mapping the physical properties directly. The Gaussian mean is set to the photon’s surface position: $\boldsymbol{\mu}_i \leftarrow \mathbf{x}_p$, and the Gaussian flux is set to the photon’s flux: $\Phi_i \leftarrow \Delta\Phi_p$. Rotation \mathbf{q}_i and scale \mathbf{s}_i have no direct analog in a discrete particle. We therefore randomly initialize \mathbf{q}_i and set the initial \mathbf{s}_i to a small, isotropic value, providing diverse local support for subsequent optimization. Through gradient-based optimization, orientations and scales will align with dominant light paths. This *particle-to-field* process (illustrated in Figure 3) results in a continuous, differentiable field, setting the stage for gradient-based optimization and efficient, reusable radiance queries.

4.2 Differentiable Radiance Querying

During training and inference, rendering proceeds by tracing camera rays through the scene for radiance estimation, querying the Gaussian photon field, which encodes the spatial distribution of photon energy. This design replaces discrete photon-based estimation with a continuous radiance function, allowing radiance to be evaluated directly from the learned Gaussian field without repeated tracing. This section describes our hybrid ray tracing pipeline (Sec. 4.2) and the radiance query mechanism (Sec. 4.2).

Ray Tracing with Gaussian Radiance Integration. We employ a path-tracing-style camera integrator augmented with Gaussian radiance field queries for diffuse interactions. Given a camera ray $\mathbf{r}(t) = \mathbf{o} + t\mathbf{d}$, the outgoing radiance

is computed by the rendering equation:

$$L_o(\mathbf{x}, \omega_o) = L_e(\mathbf{x}, \omega_o) + \int_{\Omega} f_r(\mathbf{x}, (\omega_o^i)) L_i(\mathbf{x}, \omega_i) |\cos \theta_i| d\omega_i, \quad (4)$$

where $L_i(\mathbf{x}, \omega_i)$ is approximated by $L_{\text{GPF}}(\mathbf{x}, \omega_i)$.

Our algorithm follows the standard path-tracing loop but introduces a key modification at diffuse interactions. When a view ray first encounters a diffuse surface, instead of spawning further secondary rays or gathering photons, we query GPF to obtain the preaccumulated incident radiance. This hybrid design drastically reduces variance and avoids double-counting BSDF contributions, as the radiance stored in the field already encodes the expected reflected contribution from photon sampling during optimization. The accumulated radiance at a diffuse surface point \mathbf{x} is thus:

$$L(\mathbf{x}) = L_e(\mathbf{x}) + \beta L_{\text{GPF}}(\mathbf{x}), \quad (5)$$

where β denotes the current throughput. For specular or glossy interactions with probability $p(\omega_o)$ of sampling the direction ω_o , we continue the path tracing as:

$$\beta \leftarrow \beta \cdot \frac{f_r(\mathbf{x}, (\omega_o^i)) |\cos \theta_i|}{p(\omega_o)}. \quad (6)$$

This hybrid formulation preserves physical correctness for specular transport while amortizing diffuse transport via the learned Gaussian radiance. As shown in Figure 3, camera rays propagate through the scene: specular and glossy bounces use classical path tracing, while diffuse bounces query the Gaussian field for fast radiance estimation.

Radiance Query and Aggregation. Given a surface query point \mathbf{x} (first diffuse hit) with outgoing direction ω_o toward the viewer, we gather contributions from a spatial neighborhood $\mathcal{N}(\mathbf{x})$ of nearby Gaussians. The GPF aggregated radiance is computed as:

$$L_{\text{GPF}}(\mathbf{x}, \omega_o) = \sum_{i \in \mathcal{N}(\mathbf{x})} w_i(\mathbf{x}) \Phi_i, \quad (7)$$

$$\text{with } w_i(\mathbf{x}) = \exp\left(-\frac{1}{2}(\mathbf{x} - \boldsymbol{\mu}_i)^\top \boldsymbol{\Lambda}_i (\mathbf{x} - \boldsymbol{\mu}_i)\right) \cdot \psi(\|\mathbf{x} - \boldsymbol{\mu}_i\|), \quad (8)$$

i.e., with $w_i(\mathbf{x})$ an anisotropic Gaussian kernel modulated by a smooth distance falloff, as spatial weight; and $\psi(\cdot)$ a soft attenuation that decays near a maximum radius r_{max} to ensure stability and avoid hard boundaries. The BSDF term f_r modulates the field query by the surface reflectance properties, ensuring that Gaussian primitives Φ_i encode a base radiance field that is view-independent, while the final radiance L_{GPF} correctly accounts for directional reflectance. All terms are differentiable w.r.t. $(\boldsymbol{\mu}_i, \mathbf{q}_i, \mathbf{s}_i, \Phi_i)$, enabling end-to-end optimization.

Neighborhood Search. To balance efficiency and adaptivity, we employ a hybrid spatial retrieval strategy:

$$\mathcal{N}(\mathbf{x}) = \text{BallQuery}(\mathbf{x}, r) \cup \text{kNN}(\mathbf{x}, \max(0, k_{\text{min}} - k_r)). \quad (9)$$

I.e., for dense photon regions, we perform a radius-based query using a KD-tree (BallQuery), returning k_r Gaussians. In sparse regions, where $k_r < k_{\min}$ neighbors are found, we supplement with a k-nearest-neighbor (kNN) query to guarantee coverage. This ensures consistent density support while maintaining smooth transitions.

Differentiable Accumulation. All query components—including anisotropic weighting, soft distance attenuation, and normalization—are differentiable w.r.t. Gaussian parameters $(\boldsymbol{\mu}, \mathbf{q}, \mathbf{s}, \boldsymbol{\Phi})$. Implementation relies on `Dr.Jit` [16] with full GPU vectorization, aggregating per-neighborhood contributions via a parallel scatter-reduce. This enables efficient batched training and stable gradient-based optimization, supporting fast radiance evaluation once the field is trained without relying on non-differentiable lookups or per-view kernel density estimation.

4.3 Supervision and Training

The Gaussian photon field is trained under sparse multi-view supervision derived from physically-based progressive photon mapping [12]. Instead of supervising at the image level, we operate at the level of *first-bounce diffuse surface points*—that is, the surface intersections where camera rays first hit diffuse materials. This design ensures precise geometric alignment between the queried radiance and ground-truth locations, while excluding background and invalid samples.

Ground-truth Generation. For each of the k training camera views, we gather the set of diffuse surface points visible from the camera: $\mathcal{V} = \{\mathbf{x}_i \in \mathcal{D} \mid \exists \gamma \in \mathcal{P}(o, \mathbf{x}_i) : \text{NonDiffuse}(\gamma, \mathcal{S} \setminus \mathcal{D}) \wedge \text{FirstDiffuse}(\gamma, \mathcal{D})\}$, where o is the camera position, \mathcal{S} is the full scene geometry, $\mathcal{D} \subset \mathcal{S}$ is the diffuse subset, and $\mathcal{P}(o, \mathbf{x})$ denotes the set of all finite piecewise-linear paths from o to \mathbf{x} . The predicate $\text{NonDiffuse}(\gamma, \mathcal{S} \setminus \mathcal{D})$ is true if each intermediate point of γ lies on a non-diffuse surface, including both specular and glossy interactions, and $\text{FirstDiffuse}(\gamma, \mathcal{D})$ is true if the path first intersects a diffuse point at its endpoint.

For every supervision point $\mathbf{x} \in \mathcal{V}$, the ground-truth radiance is computed using a high-quality Stochastic Progressive Photon Mapping (SPPM) reference. Although generating these references is computationally expensive, it is performed only once for training; once optimized, our field enables fast, reusable radiance queries for arbitrary novel views. Following the standard SPPM procedure, photons are traced from light sources and stored only on diffuse surfaces during each iteration. The radiance at \mathbf{x} is then estimated by gathering nearby photons and averaging across N_{iter} progressive iterations:

$$L_{\text{ref}}(\mathbf{x}, \omega_o) = \frac{1}{N_{\text{iter}}} \sum_{t=1}^{N_{\text{iter}}} \frac{1}{\pi r_t^2} \sum_{\mathbf{p}_i \in \mathcal{B}_t(\mathbf{x})} \Phi_i \cdot f_r(\mathbf{x}, \omega_i, \omega_o), \quad (10)$$

where ω_i is the photon incident direction, ω_o the camera viewing direction, $\mathcal{B}_t(\mathbf{x})$ the photon neighborhood within radius r_t , Φ_i the photon power, and f_r the BSDF [12, 30]. This yields a low-variance, physically-accurate estimate of the directional outgoing radiance at \mathbf{x} .

Training. During optimization, we trace camera rays for the same k reference views and query the photon field at each *first diffuse surface intersection* to obtain predicted radiance $L_{\text{GPF}}(\mathbf{x})$. The field parameters are optimized by minimizing a mean-squared error (MSE) loss in radiance space:

$$\mathcal{L}_{\text{MSE}} = \frac{1}{|\mathcal{V}|} \sum_{\mathbf{x} \in \mathcal{V}} \|L_{\text{GPF}}(\mathbf{x}, \omega_o) - L_{\text{ref}}(\mathbf{x}, \omega_o)\|_2^2. \quad (11)$$

5 Experiments

We validate our method on our newly-proposed challenging benchmark, comparing to both classical physically-based integrators and standard neural rendering approaches and justifying design choices via multiple ablation studies.

5.1 Experimental Setup

Datasets. Since no standard or well-established datasets exist for this task, we propose a new one consisting of five physically-based rendering scenes that cover a wide range of light-transport phenomena, including specular–diffuse interactions, caustics, and glossy reflections:

- *Veach-Bidir* and *Veach-Ajar*: classic Mitsuba-3-compatible test scenes from Bitterli’s rendering resources [3], featuring multi-bounce specular–diffuse paths and complex indirect illumination.
- *Water-Caustic* and *Water-Caustic 2*: scenes inspired by [3] and reconfigured for Mitsuba 3, with challenging refractive and specular–diffuse caustics.
- *Cornell Box* [17]: canonical diffuse reference scene to evaluate radiometric accuracy and convergence behavior.

Training Protocol. The model is trained with per-pixel final radiance from SPPM, using only 3 views and 1024×1024 radiance maps for all scenes except *Veach-Bidir* (30 views, 720×1280 maps). See the appendix for more details.

5.2 Quantitative Comparisons and Ablation Studies

Comparison with Baselines. Table 1 compares GPF against physically-based integrators (path/particle tracing [17], SPPM [12]), Gaussian mixture modeling (EM-GMM [15]), and feed-forward neural rendering (RenderFormer [46]). For EM-GMM, we reproduce the method in Mitsuba 3 as no public code is available. For RenderFormer, we use the official code and convert our scenes to their format.

The results show that GPF achieves the highest overall performance across all metrics (PSNR [7], SSIM [40], LPIPS [48]). In scenes dominated by indirect lighting (*Veach-Bidir*, *Veach-Ajar*), our method significantly surpasses all baselines in both SSIM and LPIPS, demonstrating its ability to capture smooth, high-frequency radiance variations while maintaining global consistency. For caustic-dominated scenes (*Water-Caustic*, *Water-Caustic 2*), GPF achieves the best

Table 1: Comparison across 5 complex scenes, reporting PSNR, SSIM, LPIPS, and storage cost (in MB). **Best** and **2nd best** results are highlighted.

Method	<i>Veach-Bidir</i>				<i>Veach-Ajar</i>				<i>Water-Caustic</i>			
	PSNR↑	SSIM↑	LPIPS↓	Storage↓	PSNR↑	SSIM↑	LPIPS↓	Storage↓	PSNR↑	SSIM↑	LPIPS↓	Storage↓
Path Tracer 10 spp	16.01	0.134	0.778	–	9.276	0.098	0.651	–	12.09	0.221	0.663	–
Path Tracer 50 spp	19.90	0.224	0.716	–	15.21	0.242	0.531	–	12.86	0.319	0.573	–
Particle Tracer 64 spp	25.29	0.587	0.365	–	14.19	0.240	0.750	–	12.31	0.542	0.476	–
SPPM - 3 it	18.01	0.146	0.696	26.49	14.58	0.314	0.516	405.3	26.53	0.664	0.413	14.16
EM-GMM	13.52	0.095	0.823	–	8.14	0.072	0.708	–	12.39	0.185	0.702	–
RenderFormer	14.23	0.108	0.812	–	8.56	0.081	0.692	–	11.34	0.198	0.695	–
GPF (Ours)	37.61	0.926	0.338	18.33	25.84	0.691	0.324	267.2	27.12	0.936	0.158	9.724
Method	<i>Water-Caustic 2</i>				<i>Cornell Box</i>				Mean			
	PSNR↑	SSIM↑	LPIPS↓	Storage↓	PSNR↑	SSIM↑	LPIPS↓	Storage↓	PSNR↑	SSIM↑	LPIPS↓	Storage↓
Path Tracer 10 spp	11.88	0.248	0.637	–	30.49	0.654	0.497	–	15.95	0.271	0.645	–
Path Tracer 50 spp	12.24	0.304	0.579	–	34.59	0.850	0.403	–	18.96	0.388	0.560	–
Particle Tracer 64 spp	12.08	0.528	0.489	–	33.89	0.820	0.370	–	19.55	0.543	0.490	–
SPPM - 3 it	25.64	0.632	0.412	16.26	30.47	0.754	0.399	21.63	23.05	0.502	0.487	96.77
EM-GMM	10.47	0.192	0.688	–	13.26	0.205	0.558	–	11.56	0.150	0.696	–
RenderFormer	10.92	0.210	0.672	–	32.14	0.738	0.452	–	15.44	0.267	0.665	–
GPF (Ours)	28.72	0.962	0.196	12.34	39.73	0.936	0.183	15.46	31.80	0.890	0.240	64.61

PSNR and substantially outperforms others in SSIM and LPIPS, highlighting its capacity to accurately model concentrated photon energy distributions through the learned continuous field. While PSNR is a pixel-wise metric sensitive to small local deviations, our method preserves perceptual and structural fidelity much better, as reflected by large gains in SSIM and LPIPS. Even on the simple *Cornell Box*, GPF consistently outperforms all baselines across metrics, confirming its robustness and general applicability to diverse light transport phenomena.

We further compare against two methods that represent alternative paradigms for accelerating radiance computation, but both fail on our scenes. EM-GMM [15], the only prior method applying Gaussian mixtures to photon-based light transport, serves as the most directly relevant baseline. However, its volumetric kernel normalization ($\int G(\mathbf{x}) dV = 1$) does not hold for photons deposited on surfaces, resulting in incorrect radiance estimates (see Sec. 2 for a detailed discussion). RenderFormer [46] represents the feed-forward neural rendering paradigm, sharing GPF’s motivation of replacing repeated computation with a learned mapping. However, it is trained exclusively on opaque materials and cannot handle transparency or refraction, precluding caustics. These failures underscore that complex light transport demands physics-grounded representations rather than purely statistical or data-driven alternatives.

Comparison with Neural Scene Representations. To contextualize GPF within the broader paradigm of continuous scene representations, we compare it with neural radiance field methods such as Instant-NGP [29], 3DGS [23], and AnySplat [20] in Table 2. We emphasize that this comparison is not intended as an equal-input benchmark. Neural baselines operate under fundamentally different assumptions: they rely solely on RGB images and camera poses, and primarily optimize for appearance reconstruction. In contrast, GPF assumes access to scene geometry, materials, and lighting, and explicitly models physically grounded light transport. Our goal in this comparison is con-

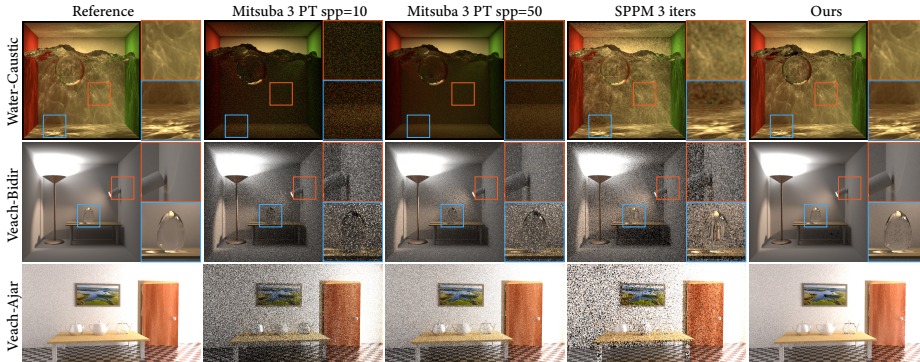


Fig. 4: Qualitative comparison results. We compare GPF with path tracing and *SPPM* on scenes with complex indirect illumination and caustics. Our method yields cleaner results with fewer noise artifacts and more accurate light transport, especially in challenging caustic and multi-bounce diffuse regions. Please  zoom in for details.

Table 2: Comparison with Instant-NGP, 3DGS, AnySplat on caustic scenes, with varying training view numbers. **Best** and **2nd best** results are highlighted.

Method	<i>Water-Caustic</i>			<i>Water-Caustic 2</i>		
	PSNR \uparrow	SSIM \uparrow	LPIPS \downarrow	PSNR \uparrow	SSIM \uparrow	LPIPS \downarrow
Instant-NGP [29] - 3 views	13.42	0.466	0.748	13.09	0.460	0.734
Instant-NGP [29] - 10 views	12.59	0.473	0.618	12.44	0.480	0.620
3DGS [23] - 3 views	16.76	0.508	0.493	17.80	0.550	0.485
3DGS [23] - 10 views	26.58	0.812	0.246	26.44	0.843	0.244
AnySplat [20] - 3 views	17.24	0.522	0.476	18.35	0.572	0.468
AnySplat [20] - 10 views	26.83	0.825	0.238	26.71	0.858	0.235
GPF (Ours) - 3 views	27.12	0.936	0.158	28.72	0.962	0.196

ceptual rather than competitive: to evaluate whether purely appearance-driven representations can faithfully reconstruct complex global illumination phenomena, *e.g.*, caustics and specular–diffuse transport. Even when given significantly more input views than GPF, these methods struggle to recover high-frequency and physically-consistent illumination effects under sparse supervision. This suggests that physics-grounded modeling remains essential for accurate and view-consistent reconstruction of complex light transport.

Ablation Studies. Table 3 analyzes the influence of three key components in our framework: the physically grounded initialization (w_{init}), the radius-based neighborhood weighting (w_{radius}), and the k -nearest-neighbor fallback (w_{knn}). Without initialization, Gaussian primitives are randomly sampled, and the lack of photon-based priors makes optimization unstable, often leading to suboptimal local minima. Using only w_{radius} leaves sparse regions without valid Gaussians, resulting in incomplete radiance reconstruction. Using only w_{knn} removes spatial adaptivity, producing over-smoothed illumination and weaker caustics. Combin-

NeRF (3 views) NeRF (10 views) 3DGS (3 views) 3DGS (10 views) Ours (3 views)

To view the animation, please use compatible software (*e.g.*, *Adobe Acrobat* or *KDE Okular*).

Fig. 5: Multi-view comparison on Water-Caustic 2 with NeRF and 3DGS. Unlike NeRF and 3DGS, which exhibit view-dependent artifacts under sparse supervision, Gaussian Photon Field (GPF) preserves consistent caustics and global illumination even with 3 views.

Table 3: Ablation study on different components.

w_{init}	w_{radius}	w_{knn}	PSNR \uparrow	SSIM \uparrow	LPIPS \downarrow
	✓		26.73	0.8962	0.2152
		✓	26.42	0.8847	0.2118
	✓	✓	26.90	0.9026	0.2208
✓	✓		26.93	0.9128	0.1792
✓		✓	26.97	0.9118	0.1769
✓	✓	✓	27.12	0.9355	0.1579

ing all three components yields the best performance: w_{init} provides a stable physical prior, w_{radius} ensures spatial adaptivity, and w_{knn} offers a robust fallback in sparse regions. Further ablation studies are provided in the appendix.

5.3 Qualitative Evaluation

Figure 4 presents qualitative comparisons across three representative scenes, with more exhaustive results in supplementary material. For the *Water-Caustic* scene, GPF produces sharp, accurate caustics that capture the subtle refractive patterns, while *SPPM - 3 iters* yields blurred illumination due to its limited photon budget and path tracing [17] (PT) fails to recover detailed structures even at 50 spp. In the *Veach-Bidir* scene, which features complex multi-bounce diffuse transport and glossy interreflections, GPF achieves a clean, noise-free reconstruction with well-defined highlights, unlike *SPPM - 3 iters* and path tracing, which exhibit noise and structural artifacts. Similarly, in the *Veach-Ajar* scene, GPF provides smooth, stable illumination with accurate indirect lighting, whereas other integrators suffer from high-frequency noise and incomplete light transport. Overall, GPF combines the physical accuracy of photon-based rendering with the smoothness of a continuous learned radiance field, delivering superior results for both caustic and indirect illumination.

Furthermore, as shown in Figure 5, our photon field enables strong consistency across novel viewpoints. Despite large changes in camera pose and viewing

Table 4: Rendering time (in seconds) comparison, across five scenes.

Method	<i>V-Bidir</i>	<i>V-Ajar</i>	<i>W-Caustic</i>	<i>W-Caustic 2</i>	<i>Cornell</i>
PT 10 spp	3.9	3.8	3.7	3.9	2.5
PT 50 spp	4.3	5.0	7.4	7.5	4.5
SPPM - 3 iters	23.4	42.0	26.4	24.7	32.8
SPPM - 1000 iters	7,793.3	14,010.0	8,790.0	8246.7	10,923.0
GPF (Ours)	6.3	30.1	16.34	15.3	26.7

direction, both direct and indirect lighting remain coherent, with stable caustics and diffuse shading. This highlights the robustness and view-reusability of our learned field, effectively amortizing photon-based light transport across views. Additional visualizations for all scenes are provided in the appendix.

5.4 Efficiency Analysis

Rendering Time. Table 4 compares the rendering time per image across all scenes. While the *Path Tracer* (spp=10 and spp=50) provides fast but noisy results, and *SPPM - 3 iters* yields moderate accuracy at the cost of higher computation, our method achieves comparable visual quality to the *SPPM - 1000 iters* reference while being orders of magnitude faster. Specifically, *SPPM - 1000 iters*—used only for generating the reference and final radiance ground truth—requires several hours per frame (up to 14,000 seconds), whereas GPF produces results of similar fidelity within only 6–30 seconds per image. This efficiency stems from reusing the learned radiance field across views, eliminating repeated photon tracing and progressive iterations.

Total Computational Cost. GPF requires a one-time preprocessing cost: generating ground-truth radiance maps ($2.3\text{h} \times 3 \text{ views} = 6.9\text{h}$) and training the field (5.4h), totaling approximately 12.3h. After training, rendering a novel view takes only 15s, compared to 2.3h for *SPPM - 1000 iters*. Figure 6 shows the total time as a function of the view number. Even accounting for the full preprocessing cost (GT generation + training), GPF becomes more efficient than SPPM after **6 views**, achieving $1.9\times$ speedup at 10 views and $18\times$ at 100 views. This demonstrates clear practical value for multi-view rendering scenarios such as simulation, synthetic data generation, and virtual production.

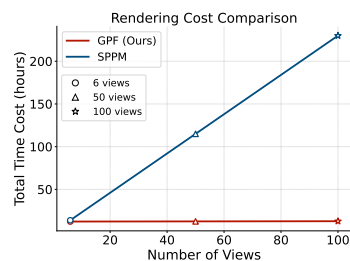


Fig. 6: Total rendering cost comparison. GPF amortizes a one-time training cost, becoming more efficient than SPPM beyond 6 views.

6 Conclusion

We introduce the Gaussian Photon Field (GPF), a physically-grounded radiance representation that unifies photon mapping and neural fields. By reformulating per-view kernel density estimation into a continuous Gaussian field, GPF enables efficient, view-reusable global illumination while preserving physical accuracy. Experiments show that GPF achieves photon-level accuracy with orders-of-magnitude faster rendering and strong multi-view consistency. This formulation bridges classical light transport simulation and learnable radiance representations, pointing toward physically accurate, differentiable rendering of dynamic and volumetric scenes. Future work will explore leveraging GPF’s efficiency and differentiability for inverse caustics.

Acknowledgements

We thank the anonymous reviewers for their insightful comments and suggestions.

References

1. Azinovic, D., Li, T.M., Kaplanyan, A., Nießner, M.: Inverse path tracing for joint material and lighting estimation. In: CVPR (2019)
2. Barron, J.T., Malik, J.: Shape, illumination, and reflectance from shading. In: TPAMI (2014)
3. Bitterli, B.: Rendering resources (2016), <https://benedikt-bitterli.me/resources/>
4. Bitterli, B., Wyman, C., Pharr, M., Shirley, P., Lefohn, A., Jarosz, W.: Spatiotemporal reservoir resampling for real-time ray tracing with dynamic direct lighting. In: TOG (2020)
5. Chen, T.H., Chan, J.W., Shiu, H.S., Yen, S.H., Yeh, C., Liu, Y.L.: Narcan: Natural refined canonical image with integration of diffusion prior for video editing. In: NeurIPS (2024)
6. Condor, J., Speierer, S., Bode, L., Bozic, A., Green, S., Didyk, P., Jarabo, A.: Don’t splat your gaussians: Volumetric ray-traced primitives for modeling and rendering scattering and emissive media. *ACM Transactions on Graphics (TOG)* **44**(1), 1–17 (Feb 2025). <https://doi.org/10.1145/3711853>, <http://dx.doi.org/10.1145/3711853>
7. Eskicioglu, A.M., Fisher, P.S.: Image quality measures and their performance. *IEEE Transactions on Communications* **43**(12), 2959–2965 (1995). <https://doi.org/10.1109/26.477498>
8. Fang, Q., Boas, D.A.: Monte carlo simulation of photon migration in 3d turbid media accelerated by graphics processing units. *Optics express* **17**(22), 20178–20190 (2009)
9. Goral, C.M., Torrance, K.E., Greenberg, D.P., Battaile, B.: Modeling the interaction of light between diffuse surfaces. In: *Proceedings of the 11th Annual Conference on Computer Graphics and Interactive Techniques*. p. 213–222. SIGGRAPH ’84, Association for Computing Machinery, New York, NY, USA (1984). <https://doi.org/10.1145/800031.808601>, <https://doi.org/10.1145/800031.808601>

10. Green, P., Kautz, J., Matusik, W., Durand, F.: View-dependent precomputed light transport using nonlinear gaussian function approximations. In: Proceedings of I3D (2006)
11. Guo, X., Sun, J., Dai, Y., Chen, G., Ye, X., Tan, X., Ding, E., Zhang, Y., Wang, J.: Forward flow for novel view synthesis of dynamic scenes (2023)
12. Hachisuka, T., Jensen, H.W.: Stochastic progressive photon mapping. *ACM Transactions on Graphics (TOG)* **28**(5), 1–8 (Dec 2009). <https://doi.org/10.1145/1618452.1618487>, <https://doi.org/10.1145/1618452.1618487>
13. Hachisuka, T., Ogaki, S., Jensen, H.W.: Progressive photon mapping. *ACM Transactions on Graphics (TOG)* **27**(5) (Dec 2008). <https://doi.org/10.1145/1409060.1409083>, <https://doi.org/10.1145/1409060.1409083>
14. Huang, B., Yu, Z., Chen, A., Geiger, A., Gao, S.: 2d gaussian splatting for geometrically accurate radiance fields. In: Special Interest Group on Computer Graphics and Interactive Techniques Conference Conference Papers '24. p. 1–11. SIGGRAPH '24, ACM (Jul 2024). <https://doi.org/10.1145/3641519.3657428>, <http://dx.doi.org/10.1145/3641519.3657428>
15. Jakob, W., Regg, C., Jarosz, W.: Progressive Expectation–Maximization for hierarchical volumetric photon mapping. *Computer Graphics Forum* **30**(4) (2011)
16. Jakob, W., Speierer, S., Roussel, N., Vicini, D.: Dr.jit: A just-in-time compiler for differentiable rendering. *Transactions on Graphics (Proceedings of SIGGRAPH)* **41**(4) (Jul 2022). <https://doi.org/10.1145/3528223.3530099>
17. Jakob, W., Speierer, S., Roussel, N., Nimier-David, M., Vicini, D., Zeltner, T., Nicolet, B., Crespo, M., Leroy, V., Zhang, Z.: Mitsuba 3 renderer (2022), <https://mitsuba-renderer.org>
18. Jensen, H.W.: Global illumination using photon maps. In: Proceedings of the Eurographics Workshop on Rendering Techniques '96. p. 21–30. Springer-Verlag, Berlin, Heidelberg (1996)
19. Jensen, H.W.: Realistic image synthesis using photon mapping. AK Peters/crc Press (2001)
20. Jiang, L., Mao, Y., Xu, L., Lu, T., Ren, K., Jin, Y., Xu, X., Yu, M., Pang, J., Zhao, F., et al.: Anysplat: Feed-forward 3d gaussian splatting from unconstrained views. *ACM Transactions on Graphics (TOG)* **44**(6), 1–16 (2025)
21. Kajiya, J.T.: The rendering equation. In: Proceedings of the 13th Annual Conference on Computer Graphics and Interactive Techniques. p. 143–150. SIGGRAPH '86, Association for Computing Machinery, New York, NY, USA (1986). <https://doi.org/10.1145/15922.15902>, <https://doi.org/10.1145/15922.15902>
22. Keller, A.: Instant radiosity. In: Proceedings of the 24th annual conference on Computer graphics and interactive techniques. pp. 49–56 (1997)
23. Kerbl, B., Kopanas, G., Leimkühler, T., Drettakis, G.: 3d gaussian splatting for real-time radiance field rendering. *ACM Transactions on Graphics (TOG)* **42**(4) (July 2023), <https://repo-sam.inria.fr/fungraph/3d-gaussian-splatting/>
24. Knaus, C., Zwicker, M.: Progressive photon mapping: A probabilistic approach. *ACM Transactions on Graphics (TOG)* **30**(3) (May 2011). <https://doi.org/10.1145/1966394.1966404>, <https://doi.org/10.1145/1966394.1966404>
25. Li, Z., Niklaus, S., Snavely, N., Wang, O.: Neural scene flow fields for space-time view synthesis of dynamic scenes. In: Proceedings of the IEEE/CVF Conference on Computer Vision and Pattern Recognition (CVPR) (2021)
26. Liu, Y.L., Gao, C., Meuleman, A., Tseng, H.Y., Saraf, A., Kim, C., Chuang, Y.Y., Kopf, J., Huang, J.B.: Robust dynamic radiance fields. In: Proceedings of the IEEE/CVF Conference on Computer Vision and Pattern Recognition (CVPR) (2023)

27. Ma, C., Liu, Y.L., Wang, Z., Liu, W., Liu, X., Wang, Z.: Humannerf-se: A simple yet effective approach to animate humannerf with diverse poses. In: Proceedings of the IEEE/CVF Conference on Computer Vision and Pattern Recognition (CVPR) (2024)
28. Mildenhall, B., Srinivasan, P.P., Tancik, M., Barron, J.T., Ramamoorthi, R., Ng, R.: Nerf: Representing scenes as neural radiance fields for view synthesis. *Communications of the ACM* **65**(1), 99–106 (2021)
29. Müller, T., Evans, A., Schied, C., Keller, A.: Instant neural graphics primitives with a multiresolution hash encoding. *ACM Transactions on Graphics (TOG)* **41**(4), 102:1–102:15 (Jul 2022). <https://doi.org/10.1145/3528223.3530127>, <https://doi.org/10.1145/3528223.3530127>
30. Nicodemus, F.E.: Directional reflectance and emissivity of an opaque surface. *Applied optics* **4**(7), 767–775 (1965)
31. Park, K., Sinha, U., Barron, J.T., Bouaziz, S., Goldman, D.B., Seitz, S.M., Martin-Brualla, R.: Nerfies: Deformable neural radiance fields. arXiv preprint arXiv:2102.07064 (2021)
32. Park, K., Sinha, U., Hedman, P., Barron, J.T., Bouaziz, S., Goldman, D.B., Martin-Brualla, R., Seitz, S.M.: Hypernerf: A higher-dimensional representation for topologically varying neural radiance fields. arXiv preprint arXiv:2106.13228 (2021)
33. Pumarola, A., Corona, E., Pons-Moll, G., Moreno-Noguer, F.: D-nerf: Neural radiance fields for dynamic scenes. In: Proceedings of the IEEE/CVF conference on computer vision and pattern recognition. pp. 10318–10327 (2021)
34. Sarrut, D., Baudier, T., Borys, D., Etxebeste, A., Fuchs, H., Gajewski, J., Grevillot, L., Jan, S., Kagadis, G.C., Kang, H.G., et al.: The opengate ecosystem for monte carlo simulation in medical physics. *Physics in Medicine & Biology* **67**(18), 184001 (2022)
35. Silverman, B.W.: Density estimation for statistics and data analysis. Routledge (2018)
36. Tretschk, E., Tewari, A., Golyanik, V., Zollhöfer, M., Lassner, C., Theobalt, C.: Nonrigid neural radiance fields: Reconstruction and novel view synthesis of a dynamic scene from monocular video. In: Proceedings of the IEEE/CVF International Conference on Computer Vision (ICCV) (2021)
37. Veach, E.: Robust monte carlo methods for light transport simulation. Ph.D. thesis, Stanford, CA, USA (1998), aAI9837162
38. Vorba, J., Karlík, O., Šik, M., Ritschel, T., Křivánek, J.: On-line learning of parametric mixture models for light transport simulation. *ACM Transactions on Graphics (TOG)* **33**(4) (2014)
39. Wang, L., Jacques, S.L., Zheng, L.: Mcm1—monte carlo modeling of light transport in multi-layered tissues. *Computer methods and programs in biomedicine* **47**(2), 131–146 (1995)
40. Wang, Z., Bovik, A.C., Sheikh, H.R., Simoncelli, E.P.: Image quality assessment: From error visibility to structural similarity. *IEEE Transactions on Image Processing (TIP)* **13**(4), 600–612 (2004). <https://doi.org/10.1109/TIP.2003.819861>
41. Wu, C.H., Chen, S.H., Hu, C.Y., Wu, H.Y., Chen, K.H., Chen, Y.Y., Su, C.H., Lee, C.K., Liu, Y.L.: Denver: Deformable neural vessel representations for unsupervised video vessel segmentation. In: Proceedings of the IEEE/CVF Conference on Computer Vision and Pattern Recognition (CVPR) (2025)
42. Xian, W., Huang, J.B., Kopf, J., Kim, C.: Space-time neural irradiance fields for free-viewpoint video. In: Proceedings of the IEEE/CVF conference on computer vision and pattern recognition. pp. 9421–9431 (2021)

43. Xu, K., Sun, W.L., Dong, Z., Zhao, D.Y., Wu, R.D., Hu, S.M.: Anisotropic spherical gaussians. *ACM Transactions on Graphics (TOG)* **32**(6) (2013)
44. Yan, L.Q., Hašan, M., Marschner, S., Ramamoorthi, R.: Position-normal distributions for efficient rendering of specular microstructure. *ACM Transactions on Graphics (TOG)* **35**(4) (2016)
45. Yang, Z., Gao, X., Sun, Y., Huang, Y., Lyu, X., Zhou, W., Jiao, S., Qi, X., Jin, X.: Spec-gaussian: Anisotropic view-dependent appearance for 3d gaussian splatting (2024), preprint
46. Zeng, C., Dong, Y., Peers, P., Wu, H., Tong, X.: Renderformer: Transformer-based neural rendering of triangle meshes with global illumination. In: *ACM SIGGRAPH 2025 Conference Papers* (2025)
47. Zhang, A., Zhao, Y., Wang, S.: Illumination estimation for augmented reality based on a global illumination model. *Multimedia tools and applications* **78**(23), 33487–33503 (2019)
48. Zhang, R., Isola, P., Efros, A.A., Shechtman, E., Wang, O.: The unreasonable effectiveness of deep features as a perceptual metric. In: *Proceedings of the IEEE conference on computer vision and pattern recognition*. pp. 586–595 (2018)
49. Zhang, Y., Sun, J., He, X., Fu, H., Jia, R., Zhou, X.: Modeling indirect illumination for inverse rendering. In: *Proceedings of the IEEE/CVF Conference on Computer Vision and Pattern Recognition*. pp. 18643–18652 (2022)
50. Zhou, Y., Wu, S., Yan, L.Q.: Unified gaussian primitives for scene representation and rendering. *arXiv preprint arXiv:2406.09733* (2024)

Supplementary Material

In this supplementary material, we provide additional implementation details for reproducibility (Section A), our complete ablation study (Section B) and additional experimental results (Section C). We also include a supplementary video illustrating the multi-view rendering consistency of our Gaussian Photon Field across diverse scenes.

A Implementation Details

We implement both our baseline *Stochastic Progressive Photon Mapping* [12] and the proposed *Gaussian Photon Field (GPF)* integrator within the *Mitsuba 3* [17] rendering framework, built upon the *Dr.Jit* differentiable runtime [16]. Both integrators share the same scene interface and BSDF/geometry infrastructure, allowing direct performance and quality comparison.

A.1 SPPM Integrator

Our baseline follows the standard formulation of stochastic progressive photon mapping [12] ([Algorithm S1](#)), consisting of alternating *photon tracing* and *camera ray tracing* stages. Each iteration emits N_p photons from all light sources

and stores them in a KD-tree for radiance estimation. The photon radius r_t is updated after each iteration according to

$$r_{t+1} = r_t \sqrt{\frac{t + \alpha}{t + 1}}, \quad (12)$$

where $\alpha = 0.7$ controls the blending rate between old and new photon contributions. For the experiments, we run $T = 1000$ iterations to produce the ground-truth reference radiance L_{ref} .

A.2 GPF Integrator

The GPF integrator extends the SPPM pipeline by replacing the per-view kernel density estimation (KDE) stage with a continuous, learnable Gaussian Photon field. We initialize a set of $M = N_p = 100,000$ anisotropic Gaussian primitives from the first SPPM iteration’s photon map, using the photon position as the mean $\boldsymbol{\mu}_i$, initial scale $\mathbf{s}_i = 0.01$, and random orientation \mathbf{q}_i . Each Gaussian stores the photon flux Φ_i as its radiance contribution.

During training, camera rays are traced through the scene using a hybrid path tracing integrator (Algorithm S2). At each diffuse surface intersection \mathbf{x} , we query nearby Gaussians within a radius $r = 0.02$ or $k = 3$ nearest neighbors using a *hybrid radius+kNN* search (Algorithm S3).

Algorithm Algorithm S1: Stochastic Progressive Photon Mapping (SPPM) baseline has three stages: (1) photon tracing to build KD-tree, (2) camera pass with KDE-based radiance gathering at first diffuse hits, and (3) progressive radius reduction following $r_{t+1} = r_t \sqrt{\frac{t+\alpha}{t+1}}$. SPPM is used as a baseline and our ground truth generator (with $T = 1000$ iterations).

```

1 def sppm(scene, camera, light, T, Np, r0=0.02, alpha=0.7):
2     L_accum, rt = 0.0, r0
3     for t in range(T):
4         # 1) Photon tracing: emit Np photons and build KD-
5             tree
6         P = PHOTON_TRACE(scene, light, Np) # store
7             (pos, flux, wi) on diffuse surfaces
8         KDT = BUILD_KDTREE(P)
9
10        # 2) Camera pass: first diffuse hit uses KDE (
11            radius-r_t gathering)
12        L_frame = 0.0
13        for pix in camera:
14            ray = PRIMARY_RAY(camera, pix)
15            hit, beta, prev_delta = TRACE_TO_FIRST_DIFFUSE
16                (scene, ray)
17            if hit is None:
18                L_frame += 0.0; continue
19            if prev_delta and IS_EMITTER(hit):

```

```

16         L_frame += beta * EMITTER_RADIANCE(hit);
           continue
17         N = RADIUS_QUERY(KDT, hit.x, rt)
18         Lp = KDE_GATHER(N, hit) # radiance:
            $L_p = \frac{1}{\pi r_t^2} \sum \Phi_j f_r$ 
19         L_frame += beta * Lp
20
21         # 3) Progressive radius update
22         rt = r0 * ((t + alpha) / (t + 1))**0.5
23         L_accum += L_frame
24     return L_accum / T

```

where w_i is the anisotropic Gaussian weight and $\epsilon = 10^{-6}$ ensures stability. Queries are implemented using a KD-tree structure built from Gaussian centers, rebuilt periodically as positions are optimized.

We only supervise **visible surface points** collected from K camera views ($K = 3-30$ depending on the scene). Each visible point’s ground-truth radiance $L_{GT}(\mathbf{x})$ is obtained from the reference SPPM after 1000 iterations.

We train the field by minimizing the MSE loss

$$\mathcal{L} = \frac{1}{N} \sum_{\mathbf{x}} \|L_{GPF}(\mathbf{x}) - L_{ref}(\mathbf{x})\|_2^2, \quad (13)$$

where N is the number of visible surface points, using the Adam optimizer with a learning rate of 5×10^{-4} . Training is performed for 10k iterations, each sampling a random subset of visible points from randomly selected views.

Algorithm Algorithm S2: Camera ray tracing with Gaussian queries. At diffuse surfaces, we query the radiance from GPF, multiply by the BSDF, and terminate. Specular/glossy segments are traced explicitly.

```

1 def render_with_gpf(scene, camera, G, r_query=0.02, k_min
   =3, kd_tree):
2     """
3     Differentiable camera pass that reuses the learned
   Gaussian field.
4     Query occurs only at diffuse surfaces; specular/glossy
   bounces are traced.
5     """
6     L_img = zeros_like(camera.pixels)
7     for pix in camera.pixels:
8         ray = generate_camera_ray(camera, pix)
9         L_pix, beta, prev_delta = 0.0, 1.0, True
10        while True:
11            hit = intersect(ray, scene)
12            if not hit: break
13
14            if is_emitter(hit) and prev_delta:
15                L_pix += beta * emitter_radiance(hit, ray.
   dir)

```

```

16         break
17
18         wo, fs, pdf, bsdf_type = sample_bsdf(hit,
19         return_type=True)
20
21         if is_diffuse(bsdf_type):
22             # Query learned radiance field and
23             # multiply by BSDF
24             Li = query_gaussian_radiance(
25             hit.position, wo, G, kd_tree,
26             r_query, k_min)
27             Lg = Li * fs # Apply BSDF modulation
28             L_pix += beta * Lg
29             break # terminate at first diffuse
30         else:
31             beta *= fs / pdf
32             prev_delta = is_delta(bsdf_type)
33             ray = spawn_ray(hit, wo)
34
35     L_img[pix] = L_pix
36     return L_img

```

All differentiable operations (Gaussian weighting and gradient accumulation) are implemented in Dr. Jit [16] with full GPU vectorization.

Algorithm Algorithm S3: Hybrid Gaussian radiance query. We first use a radius query to preserve locality and supplement with kNN to avoid empty neighborhoods. A soft normalization by $\max(\sum w_i, \epsilon)$ ensures stability.

```

1 def query_gaussian_radiance(x, view_dir, G, kd_tree, r
2 =0.02, k_min=3, eps=1e-6):
3     """
4     x:         surface point (query)
5     view_dir: outgoing direction (to camera)
6     G:         Gaussian params [(mu, sigma, quat, color),
7     ...]
8     kd_tree:   built over {mu}
9     r:         radius for ball query (default: 0.02)
10    k_min:      minimal neighbors guaranteed by kNN
11                supplement (default: 3)
12    returns:    radiance estimate at x
13    """
14    # Phase 1: radius query
15    idx_r = kd_tree.ball_query(x, r)
16    # Phase 2: supplement with kNN if sparse
17    if len(idx_r) < k_min:
18        idx_knn = kd_tree.knn_query(x, k_min)
19        idx = dedup(idx_r + idx_knn)
20    else:
21        idx = idx_r
22    # Phase 3: accumulate weighted contributions

```

Table S1: Ablation study on the number of Gaussian primitives.

# Gaussians	PSNR \uparrow	SSIM \uparrow	LPIPS \downarrow	Time (s) \downarrow
10K	24.32	0.8521	0.2847	7.230
50K	26.18	0.8892	0.2156	12.70
100K	27.12	0.9355	0.1579	16.37
200K	27.25	0.9403	0.1564	24.35

Table S2: Ablation study on the k-NN parameter k .

k	PSNR \uparrow	SSIM \uparrow	LPIPS \downarrow	Time (s) \downarrow
1	25.87	0.8756	0.2314	16.21
3	27.12	0.9355	0.1579	16.37
5	27.18	0.9372	0.1574	16.48
10	27.08	0.9342	0.1595	16.34

```

20 L = 0.0
21 Z = 0.0
22 for j in idx:
23     mu, sigma, quat, color = G[j]
24     R = quat_to_matrix(quat)           # 3x3
25     d = x - mu
26     dL = R.T @ d                       # to local frame
27     dn = (dL[0]/sigma[0], dL[1]/sigma[1], dL[2]/sigma
28           [2])
29     w_gauss = exp(-0.5 * dot(dn, dn))   #
30     # anisotropic kernel
31     # soft distance falloff (smooth outside r)
32     dist = norm(d)
33     if dist <= r:
34         w_dist = 1.0
35     else:
36         t = (dist - r) / max(r, 1e-6)
37         w_dist = exp(-3.0 * t * t)
38     w = w_gauss * w_dist
39     L += color * w
40     Z += w
41 return L / max(Z, eps)

```

B Ablation Study

Ablation on Different Number of Gaussian Primitives. Table S1 investigates the effect of varying the number of Gaussian primitives. Increasing the number of Gaussians consistently improves image quality, as reflected by higher

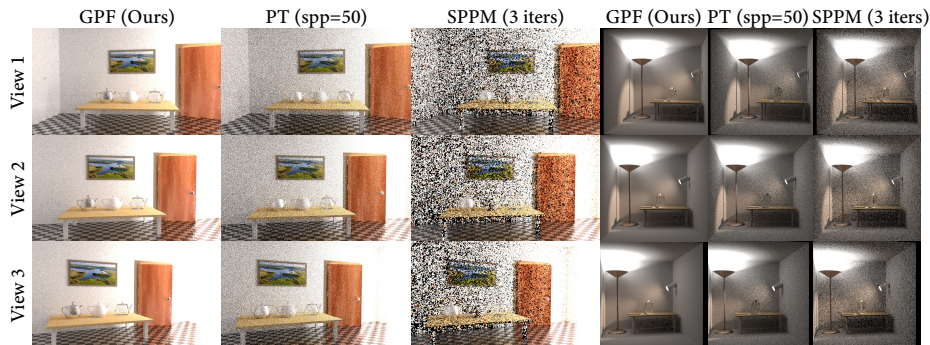


Fig. S1: Multi-view rendering results. We compare our solution with *Mitsuba 3 Path Tracer* [17], *SPPM* [12], *3DGS* [23] and *Instant-NGP* [29] across water-caustic. Our method produces cleaner results with significantly fewer noise artifacts and more accurate light transport, especially in challenging caustic. Please  zoom in for more details.

PSNR/SSIM and lower LPIPS, owing to denser photon coverage and finer radiance approximation. However, beyond 100K primitives, the performance gain becomes marginal while rendering time increases notably. We therefore adopt 100K Gaussians as a balanced configuration between quality and efficiency.

Ablation on Different k -NN Parameter. Table S2 analyzes the influence of the k -nearest-neighbor parameter on radiance aggregation. A too small k (e.g., $k=1$) leads to unstable estimation and higher noise due to insufficient photon support, while an excessively large k oversmooths high-frequency lighting and caustic details. The overall performance remains stable for k between 3 and 5, showing nearly identical image quality and computation time. We adopt $k=3$ as our default setting for its robustness and simplicity.

C Additional Experiment Results

We also provide a supplementary video demonstrating the multi-view rendering consistency across all scenes.

Multi-View Rendering Results on Veach-Ajar and Veach-Bidir. We present multi-view rendering results on the *Veach-Ajar* and *Veach-Bidir* scenes from three viewpoints (Figure S1). Our method is compared with Path Tracing (50 spp) and SPPM (3 iterations). The results demonstrate that our approach produces cleaner images with reduced noise and more stable indirect illumination across views compared to both baselines.

Multi-View Rendering Results on Water-Caustic. We present multi-view rendering results on the *Water-Caustic* (Figure S2) scene using four viewpoints. We compare our method with 3DGS under both *3-view* and *10-view* supervision, as well as with Path Tracing (50 spp) and SPPM (3 iterations). The results indicate that our method achieves sharper caustic structures, reduced noise

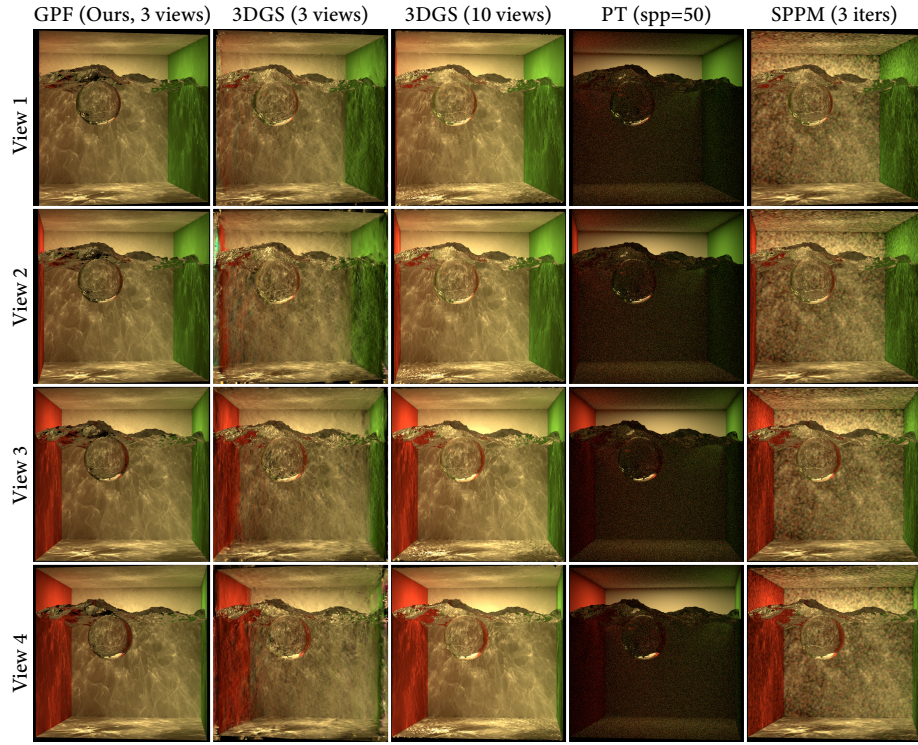


Fig. S2: Multi-view rendering results. We compare our solution with *Mitsuba 3 Path Tracer* [17], *SPPM* [12], *3DGS* [23] across water-caustic. Our method produces cleaner results with significantly fewer noise artifacts and more accurate light transport, especially in challenging caustic. Please  zoom in for more details.

levels, and more stable multi-view radiance behavior compared to the baseline approaches.

Multi-View Rendering Results on Water-Caustic 2. We present multi-view rendering results on the *Water-Caustic 2* scene (Figure S3), using four viewpoints. We compare our method with 3DGS and Instant-NGP under both *3-view* and *10-view* supervision, as well as with Path Tracing (50 spp) and SPPM (3 iterations). The results show that our approach produces cleaner caustics, fewer noise artifacts, and more consistent light transport across views compared to all baselines.

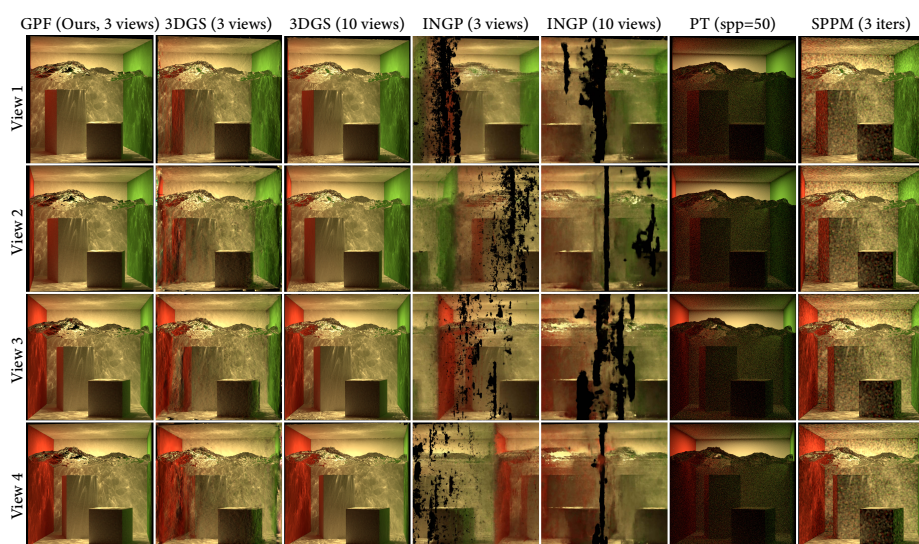


Fig. S3: Multi-view rendering results. We compare our solution with *Mitsuba 3 Path Tracer* [17], *SPPM* [12], *3DGS* [23] and *Instant-NGP* [29] across water-caustic. Our method produces cleaner results with significantly fewer noise artifacts and more accurate light transport, especially in challenging caustic. Please 🔍 zoom in for more details.